NATIONAL AERONAUTICS AND SPACE ADMINISTRATION

Technical Report 32-1504

Sizing a Solar Electric Thrust Subsystem

T. D. Masek

JET PROPULSION LABORATORY
CALIFORNIA INSTITUTE OF TECHNOLOGY
PASADENA, CALIFORNIA

November 15, 1970

NATIONAL AERONAUTICS AND SPACE ADMINISTRATION

Technical Report 32-1504

Sizing a Solar Electric Thrust Subsystem

T. D. Masek

JET PROPULSION LABORATORY
CALIFORNIA INSTITUTE OF TECHNOLOGY
PASADENA, CALIFORNIA

November 15, 1970

Prepared Under Contract No. NAS 7-100
National Aeronautics and Space Administration

Preface

The work described in this report was performed by the Propulsion Division of the Jet Propulsion Laboratory.

Contents

Tables

Figures

Abstract

The analysis presented in this report provides a simple method for determining the approximate mass and dimensions of a solar electric thrust subsystem. Each system element is discussed in terms of mass, and efficiency or power. Results are presented as a function of the power into the power conditioning units. The dependence of the size on a given mission is shown to be a function of thrust cutoff distance and thruster throttling capability.

Sizing a Solar Electric Thrust Subsystem

I. Introduction

The thrust subsystem elements, described conceptually in previous works (Refs. 1, 2), are shown schematically in Fig. 1. Elements included are thrusters, power conditioners (PC), thrust vector control (TVC), propellant storage and distribution (PSD), switching matrix (SM), and controller. All mounting structures are included in the TVC element.

Since an electric propulsion system is designed largely around the thruster, fixing the thruster size essentially establishes the designs of the remaining elements. Thus the mission dependence, for all but the PSD element, need only be considered for the thruster.

II. Mission Influence

The maximum individual thruster power level can be determined by the thrust cutoff distance and maximum thrust power. The available thrust power at any distance from the sun R can be expressed in the form (Ref. 3)

$$P_t(R) = \frac{\eta_s P_1 S}{R^2} \tag{1}$$

where

P_t = thrust power at distance R, kW

P_1 = nominal solar array power output at 1 AU, kW

R = distance between sun and probe, AU

η_s = efficiency factor of solar array

The efficiency factor η_s accounts for array power losses (e.g., cabling resistance and cell matching) and expected degradation from radiation damage. The factor S accounts for the expected change in solar cell efficiency with temperature changes and can be expressed in the form

$$S = \frac{1}{R^{3/2}}(2.17 - 7.88\,R^{1/2} + 7.51\,R - 0.80\,R^{3/2}) \tag{2}$$

This equation applies for R between 0.6 and 5 AU. A point of maximum power is expected near 0.6 AU (Ref. 3).

If the constraint is imposed that all thrusters be identical, for power matching, i.e., utilization of all available

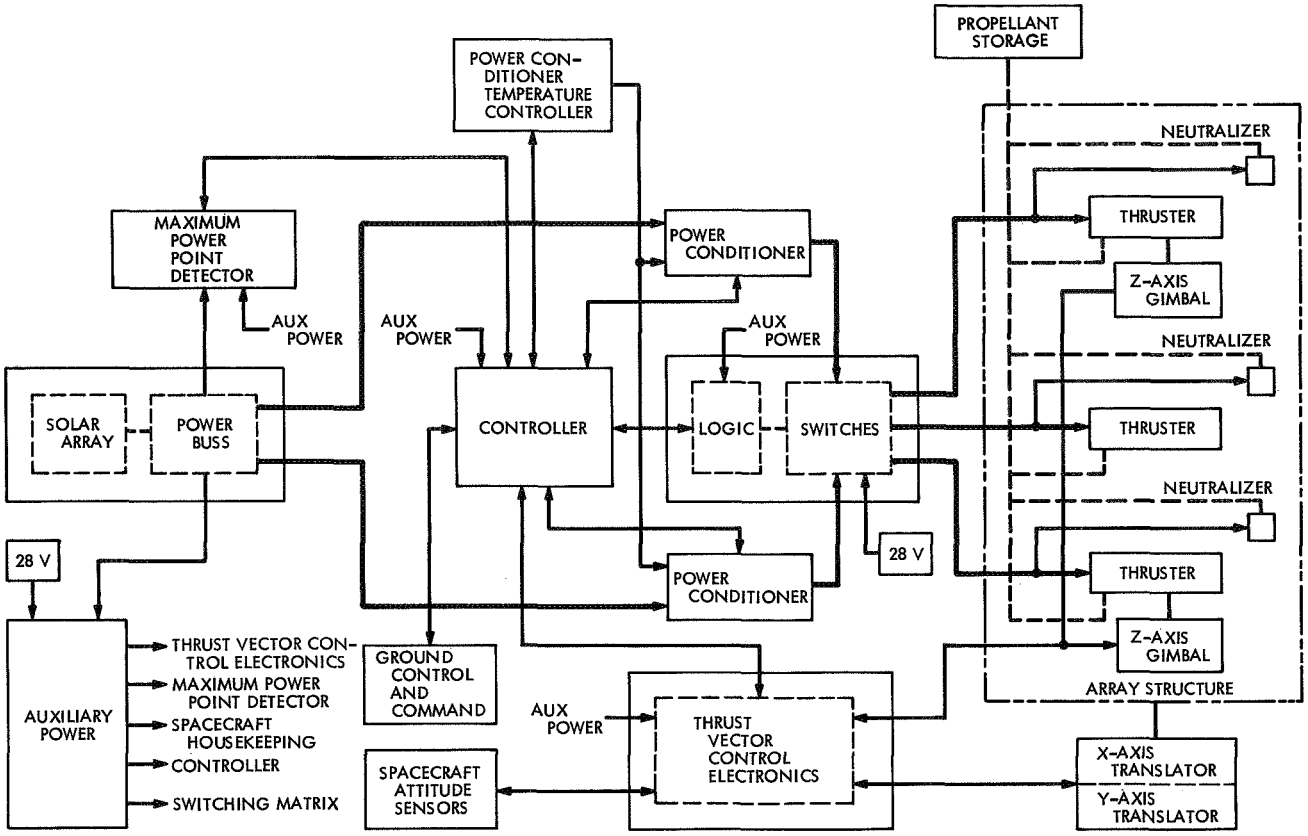

Fig. 1. Solar electric propulsion system

solar power by the thrust subsystem, the minimum number of thrusters operating at the point of minimum power is given by the smallest integer n that satisfies

$$n \geqq \frac{1}{\alpha_t - 1} \tag{3}$$

provided $S/R^2 < 1/\alpha_t$; otherwise $n = 1$. The throttling factor α_t is the ratio of thruster full power to lowest operable power. The limit on minimum operating power, hence on α_t, is determined by thruster characteristics. Thruster throttling will be discussed in Section III-A.

The minimum number of identical thrusters operating at the point of maximum power is then given by the smallest integer k that satisfies

$$k \geqq \frac{P_{\max}}{P_{\min}} \left(\frac{n}{\alpha_t}\right)$$

or

$$k \geqq \left(\frac{S}{R^2}\right)_{\max} \left(\frac{R^2}{S}\right)_{\min} \frac{n}{\alpha_t} \tag{4}$$

The maximum power level p_t of the individual thruster is then given by

$$p_t = \frac{P_{\max}}{k}, \text{kW} \tag{5}$$

If nonidentical thrusters are used, Eqs. (3) and (4) must be modified. The minimum number of nonidentical thrusters operating at the point of maximum power can be determined as follows. It is assumed that α_t is the same for all thruster sizes. The maximum power of the last (m^{th}) thruster is

$$p_m = \alpha_t P_{\min} \tag{6}$$

where $P_{\min}$ is the power at thrust cutoff. At the point where the next-to-last thruster is shut off and the last thruster is returned to full power,

$$\frac{(p_{m-1} + p_m)}{\alpha_t} = p_m$$

This gives

$$p_{m-1} = (\alpha_t - 1)\, p_m = \alpha_t (\alpha_t - 1)\, P_{\min}$$

Similarly,

$$p_{m-2} + p_{m-1} + p_m = \alpha_t (p_{m-1} + p_m)$$

so

$$p_{m-2} = \alpha_t^2 (\alpha_t - 1) P_{\min}$$

Thus, in general,

$$p_{m-1} = (\alpha_t - 1) \alpha_t^i P_{\min} \tag{7}$$

The maximum power can now be expressed in the form

$$P_{\max} \leqq \sum_{i=1}^{m} p_i = \sum_{i=1}^{m-1} (\alpha_t - 1) \alpha_t^{m-i} P_{\min} + \alpha_t P_{\min}$$

or

$$P_{\max} \leqq (\alpha_t - 1) P_{\min} \sum_{i=1}^{m-1} \alpha_t^{m-i} + \alpha_t P_{\min}$$

This simplifies to

$$P_{\max} \leqq \alpha_t^m P_{\min} \tag{8}$$

The minimum number of nonidentical thrusters is now given by the smallest integer m that satisfies the equation

$$m \geqq \frac{\log \frac{P_{\max}}{P_{\min}}}{\log \alpha_t} \tag{9}$$

In general, the use of nonidentical thrusters will allow the use of the minimum number of thrusters. However, this may not result in the system of minimum weight as discussed in the next section.

III. Component Analysis

A. Thruster

1. Size. Calculations based on the JPL SE-20C thruster design (Refs. 4, 5) have resulted in the following equation for thruster mass:

$$m_t = 1.85 + 57 D_b^2, \text{kg} \tag{10}$$

where

m_t = individual thruster mass, kg

D_b = ion beam diameter, m

The design maximum ion beam current density of the SE-20C thruster is 32 A/m². This value, about 30% below the maximum short-term capability of the SE-20C thruster (Ref. 6), is used in this analysis because of the present uncertainties in beam divergence and accelerator grid life. The beam diameter, using 32 A/m², can be written

$$D_b = \frac{6.30 \times 10^2}{I_{sp}} (\eta_m \eta_t p_t)^{1/2}, \text{m} \tag{11}$$

where

I_{sp} = true specific impulse, s

η_m = propellant utilization efficiency

η_t = total thruster efficiency;

$= \eta_m \eta_p$

η_p = power efficiency

p_t = maximum thruster power, kW

These parameters will be discussed in the following section. When Eqs. (10) and (11) are combined,

$$m_t = 1.85 + 2.26 \times 10^7 \frac{\eta_m \eta_t p_t}{I_{sp}^2}, \text{kg} \tag{12}$$

As noted previously, several thruster sizes (and associated PC units) could be used in a single system. The relative importance of using the minimum number of thrusters will now be shown. The total thruster mass is

$$M_t = \sum_i m_{t,i} N_{t,i} \tag{13}$$

where $m_{t,i}$ is the mass of the ith thruster and $N_{t,i}$ is the total number of ith thrusters. The total number of thrusters is given by

$$N_t = n_t + n_s$$

where

n_t = number of operating thrusters

n_s = number of initial spare thrusters

The total power into the PC unit P_c is

$$P_c = \frac{1}{\eta_c} \sum_i p_{t,i} n_{t,i} \tag{14}$$

and

$$\eta_c = \frac{1}{P_c} \sum_i \eta_{c,i} p_{c,i} n_{c,i}$$

where

$\eta_{c,i}$ = efficiency of the ith PC

η_c = average efficiency of PC

$p_{c,i}$ = power level of the ith PC

$n_{c,i}$ = number of ith PC units

With the use of Eqs. (12) and (14), the total thruster mass is given by

$$M_t = 1.85\,(n_t + n_s) + 2.26 \times 10^7 \frac{\eta_m \eta_t}{I_{sp}^2} \left(\eta_c P_c + \sum_i n_{s,i}\, p_{t,i}\right) \tag{15}$$

For systems operating in the specific impulse and power ranges of current interest (3000 to 4000 s and 5 to 20 kW), the second term in this equation dominates by a factor of 2 to 4. The import of this is that the fixed penalty associated with increasing the number of initially operating thrusters is small compared with the penalty for carrying a large number of spares. The determination of the number of spare thrusters (and their sizes) required for a system of nonidentical thrusters to achieve a given reliability is a major problem. However, it would seem intuitively that the number of spares would be minimized, for a given system reliability, if all thrusters were identical and interchangeable.

If all thrusters are of equal size,

$$\sum_i n_{s,i}\, p_{t,i} = n_s\, p_t = \eta_c P_c \frac{n_s}{n_t}$$

Thus, Eq. (15) becomes

$$M_t = 1.85\,(n_t + n_s) + 2.26 \times 10^7 \frac{\eta_m \eta_t \eta_c P_c}{I_{sp}^2} \left(1 + \frac{n_s}{n_t}\right) \tag{16}$$

In addition, Eq. (11) can now be written in terms of P_c as

$$D_b = \frac{6.30 \times 10^2}{I_{sp}} \left(\frac{\eta_m \eta_t \eta_c P_c}{n_t}\right)^{1/2} \tag{17}$$

The thruster array dimensions can now be determined. The thruster plan form area, exclusive of structure, is

$$A_t = \frac{\pi}{4}\,(n_t + n_s)\,(\gamma D_b)^2$$

where γ is the ratio of maximum thruster diameter to beam diameter (typically 1.4). The overall array plan form area, including structure and gimbal actuators, can be expressed as

$$A_a = \beta A_t = \frac{\beta \pi}{4}\,(n_t + n_s)\,(\gamma D_b)^2$$

where β is the ratio of array to thruster area. A value of β of 2.0 is typical of most packaging concepts (Refs. 7, 8). Thus, the array area can be represented approximately by

$$A_a = 3\,(n_t + n_s)\, D_b^2 \tag{18}$$

If we assume the array is formed with relative symmetry, a characteristic dimension of the array L_a is $A_a^{1/2}$ or

$$L_a = 1.7\, D_b\,(n_t + n_s)^{1/2}, \text{m} \tag{19}$$

This is equivalent to the dimensions of a square. The maximum dimension could thus be expected to be approximately

$$L_{a,\max} = 2^{1/2} L_a$$

$$= 2.4\, D_b\,(n_t + n_s)^{1/2}$$

Two examples can be noted. First, the thruster array of Ref. 7 with $D_b = 0.20$ m had an edge dimension of about 0.53 m and a diagonal dimension of about 0.71 m. If gimbal actuators 5 to 8 cm thick (typical of present designs) are included as expected, the observed dimensions are comparable with $L_a = 0.63$ and $L_{a,\max} = 0.91$ m. Second, a current design using a five-thruster array with gimbals and $D_b = 0.2$ m has an edge dimension of about 0.86 m ($L_a = 0.79$ m) and a diagonal dimension of about 1.06 m ($L_{a,\max} = 1.09$ m). Equation (19) should be sufficiently accurate for preliminary design of the TVC and structure.

In terms of power, Eq. (19) becomes

$$L_a = \frac{1.1 \times 10^3}{I_{sp}} \left[\frac{\eta_m \eta_t \eta_c\,(n_t + n_s)\, P_c}{n_t}\right]^{1/2}, \text{m} \tag{20}$$

Although only approximate, Eq. (20) shows that array dimensions are relatively independent of n_t, vary directly with $P_c^{1/2}$, and vary inversely with I_{sp}.

2. Efficiency. Thruster power efficiency is given by

$$\eta_p = \frac{V_b I_b}{V_b I_b + losses} = \frac{beam\ power}{p_t}$$

or

$$\eta_p = \frac{V_b}{V_b + \frac{p_L}{I_b}} = \frac{V_b}{V_b + \epsilon_L} \tag{21}$$

where

V_b = screen or beam voltage, V

P_L = power losses

I_b = ion beam current, A

$$= \frac{10^7 \eta_m \eta_t p_t}{I_{sp}^2}$$

ϵ_L = power losses per beam ion, V (or eV/ion)

Beam voltage and specific impulse are related by

$$V_b = 10^{-4}\left(\frac{I_{sp}}{\eta_m}\right)^2$$

Substituting this expression for V_b into Eq. (21) gives

$$\frac{1}{\eta_p} = 1 + 10^4\left(\frac{\eta_m}{I_{sp}}\right)^2 \frac{p_L}{I_b} = 1 + 10^4\left(\frac{\eta_m}{I_{sp}}\right)^2 \epsilon_L \tag{22}$$

The power losses, including the approximate fraction of ϵ_L each contributes, are shown in Table 1 (Refs. 6, 9, 10). Both oxide and hollow cathode thrusters are listed, although the latter appears to be more promising at this time. The liquid mercury cathode thruster (Ref. 11), under development at Hughes Research Laboratories, is expected to be similar to the hollow cathode thruster in terms of efficiency parameters. The liquid mercury cathode is in a slightly less-developed state in its system applicability and will not be discussed here. For an oxide cathode thruster, Eq. (22) can be written with little error, as

$$\frac{1}{\eta_p} = 1 + 10^4\left(\frac{\eta_m}{I_{sp}}\right)^2 \left[\frac{15}{I_b} + (\epsilon_d + \epsilon_c + \epsilon_a + \epsilon_n)\right] \tag{23}$$

and for a hollow cathode thruster, as

$$\frac{1}{\eta_p} = 1 + 10^4\left(\frac{\eta_m}{I_{sp}}\right)^2 \left[\frac{30}{I_b} + (\epsilon_d + \epsilon_a + \epsilon_n)\right] \tag{24}$$

Expressions for ϵ_d, ϵ_c, ϵ_a, and ϵ_n can be obtained from experimental data.

Discharge losses can be expressed approximately, for the range of η_m of interest (0.7 to 0.95), as

$$\epsilon_d = A_1\left(\frac{p}{p_t}\right)^{\beta_1} + A_2\left(\frac{1}{1-\eta_m}\right) \tag{25}$$

Typical constants A_1, A_2, and β_1 are shown in Table 2.

Table 1. Power loss summary

Power loss	Oxide cathode		Hollow cathode	
	Constant	Variable[a]	Constant	Variable[a]
Discharge	–	ε_d (0.45 ε_L)	–	ε_d (0.72 ε_L)
Cathode	–	ε_c (0.36 ε_L)	10 W	–
Accelerator	–	ε_a (0.05 ε_L)	–	ε_a (0.06 ε_L)
Magnet	10 W	–	10	–
Vaporizer(s)	5	–	10	–
Neutralizer	–	ε_n (0.06 ε_L)	–	ε_n (0.07 ε_L)

[a]Values in parentheses are approximate fractions of ε_L at full thruster power.

Table 2. Discharge loss equation constants

Constant	Oxide cathode		Hollow cathode	
	Present	Future	Present	Future
A_1, eV/ion	185	150	200	150
A_2, eV/ion	1.5	1.5	6.0	6.0
β_1	0.3	0.3	0.1	0

The accelerator loss can be expressed as

$$\epsilon_a = (V_a + V_b)\frac{I_i}{I_b} \tag{26}$$

where V_a is the accelerator voltage and I_i the current (impingement). The symbol I_i is primarily a function of I_b, aperture diameter and accelerator thickness. However, for present designs, the ratio I_i/I_b can be approximated from experimental data (Ref. 6) as (for a conventional two-grid system),

$$\frac{I_i}{I_b} = 0.01\left(\frac{p}{p_t}\right) \tag{27}$$

For a given V_b and V_a (1000 V is a good value for present designs), ϵ_a can be estimated from Eqs. (26) and (27).

Neutralizer losses are contributed by the cathode, vaporizer, and keeper elements and by beam-neutralizer coupling. Neutralizer power p_n can be written approximately as

$$p_n = \epsilon_n I_b = 15 + V_c I_b \tag{28}$$

where V_c is the coupling voltage.

Cathode losses must be considered separately for the oxide and hollow cathode thrusters. For the oxide cathode a reasonable representation is

$$\epsilon_c = \frac{1}{I_b}(100 + 15 I_d)\, f(t, \eta_m)$$

where

I_d = discharge current, A

$f(t, \eta_m)$ = function of time and η_m accounting for cathode degradation and use

The fact that this loss is relatively high and that it increases with time provides the impetus for the use of the hollow cathode (Ref. 12). The hollow cathode losses are limited to starting and keeper losses (about 10 W). Heating power (about 30 W) is required until the discharge current reaches several amperes, after which the cathode heater is shut off.

Power efficiency and total efficiency ($\eta_p\, \eta_m$) of the hollow cathode thruster can now be computed from Eq. (24) by using Eqs. (25) to (28) as a function of I_{sp} for $p/p_t = 1$. Figure 2 shows the results for η_m of 0.8 and 0.9, if we assume that V_b is adjustable. Although adjustment of V_b is of little difficulty for the thruster, the PC would require special design. Thus, Fig. 2 represents data for a number of different thrusters and PC units. Note that $\eta_m = 0.90$ results in the highest η_t below 3600 s I_{sp}. Figure 3 presents η_p for a given thruster with the variation in I_{sp} obtained by adjusting η_m. In evaluating Eq. (28), a value of I_b of unity was used. This should introduce little error since ϵ_a and ϵ_n are small.

Figure 2 and 3 are for thrusters at full power. At lower power the constant losses shown in Table 1 become a larger fraction of the total. The expected variation of η_t with thruster power level is shown in Fig. 4. Thus, for present thrusters, penalties of about 3% and 6.5% are paid for α_t values of 2 and 3, respectively.

In concluding this section, a comment on η_m is required. The neutralizer flow (plasma bridge type) contributes to η_m and must be considered in evaluating true specific impulse. Thus far, a factor of 2% in utilization is included for the neutralizer. This figure is consistent with the performance of cesium neutralizers (Ref. 12) and with recent data obtained with a mercury neutralizer (Ref. 13).

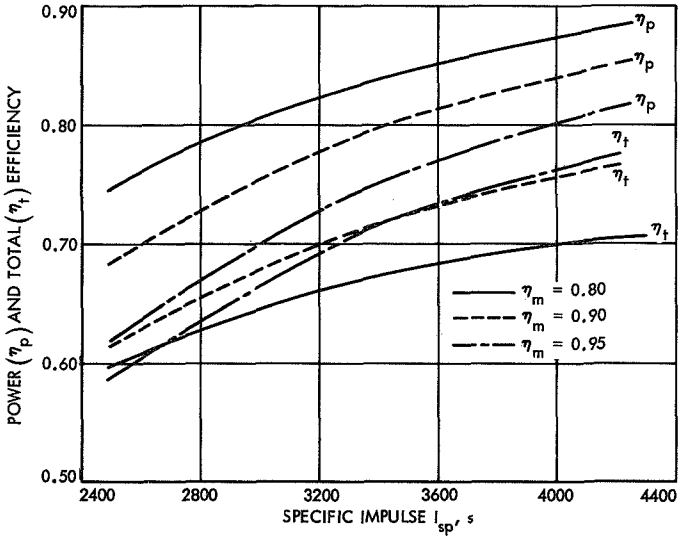

Fig. 2. Thruster power and total efficiency as a function of specific impulse

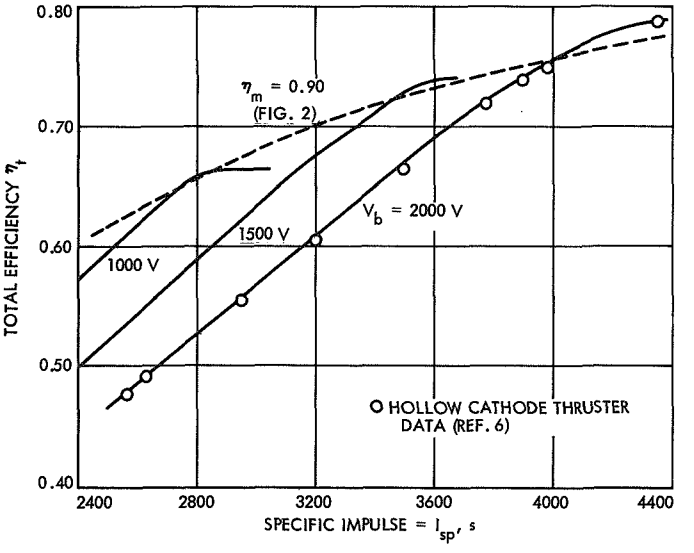

Fig. 3. Thruster total efficiency as a function of specific impulse

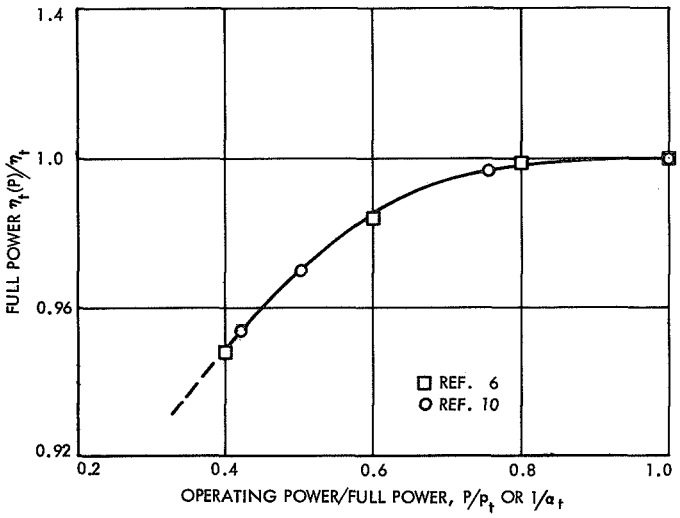

Fig. 4. Typical thruster throttling characteristics

B. Power Conditioners

1. Size. The specific mass of the PC (for a hollow cathode thruster including a neutralizer) can be approximated, from data of Refs. 8 and 14 and by

$$\frac{m_c}{p_c} = 3.8 + 7e^{-0.7p_c}\ \text{kg/kW} \tag{29}$$

The total mass is

$$M_c = \sum_i m_{c,i} N_{c,i}$$

where

$N_c = n_c + n_p$

n_c = number of operating PC units

n_p = number of initial spare PC units

For equal PCC unit size

$$M_c = (n_c + n_p)(3.8 + 7e^{-0.7p_c})\, p_c$$

$$M_c = \left(1 + \frac{n_p}{n_c}\right)(3.8 + 7e^{-0.7P_c/n_c})\, P_c, \text{kg} \tag{30}$$

The plan form area of the PC unit is required for spacecraft packaging. Present designs use direct radiation cooling and require one side of the unit to radiate to space (Ref. 9). The radiated power per unit is related to the conversion efficiency η_c by

$$p_r = (1 - \eta_c)\, p_c \tag{31}$$

A radiation flux of 400 W/m² is estimated by Ref. 8. The required area per unit is approximately

$$A_c = 0.2 + 0.2\, p_c, \text{m}^2 \tag{32}$$

Since the PC will probably be designed to fit the spacecraft, the dimensions can be adjusted as required to obtain A_c.

2. Efficiency. Accurate data on PC efficiency are not at present available. The principal difficulty in determining this efficiency is the accurate measuring of input power. Calculated efficiencies up to 93% have been predicted for transistor- and SCR-type PC units (Refs. 14, 15). The measured, full-power efficiency of the present Hughes unit (BB-1 with 40 to 80 V input from a laboratory supply) is about 89% based on input dc V–A. In the near future (through 1970) PC efficiencies of about 90% seem realistic. Higher voltage power systems (100 to 200 V) and thyristor technology should increase this efficiency into the low 90s.

In present designs using pulse width modulation with square wave inverters, the input may be pulsed (Ref. 14). This causes a ripple on the dc current and voltage. An input filter is used on the PC to minimize the input ripple. Complete ripple elimination under all line and load conditions is probably not possible without an unacceptably large filter. However, as noted in Ref. 15, the ripple frequency is expected to be high (about 160 kHz) compared with the solar array frequency response at the −3 dB point (about 30 kHz). Thus, the high frequency ripple loading is not expected to follow the array static E-I curves. This decoupling from the static curve allows operation near the maximum power point, with peak ripple power beyond the static maximum.

C. Thrust Vector Control

1. Size. The TVC will provide normal attitude control (within ±0.5 deg) of the spacecraft and will correct for thrust misalignment and spacecraft center-of-gravity changes caused by propellant depletion (Ref. 16). Three-axis control is required for this purpose. This can be accomplished by two-axis translation (of the thruster array) and thruster gimballing for systems with two or more rows of thrusters. Single-axis translation with gimballing normal to this axis may be adequate for systems with one row of thrusters. A representative single-axis translator and gimbals, described in Refs. 17 and 18, have been evaluated (Refs. 19, 20, 21). The TVC components are expected to vary only slightly with thruster size and power level.

The translation distance is determined by the requirement of maintaining control with an outboard thruster operating alone. It will be assumed that the most outboard thruster center must be translated half a thruster diameter past center. The translation distance in each direction can be written

$$L_d = \left(\frac{n_{tr}}{2} - 1\right)(\gamma D_b + \sigma) + \left(\gamma D_b + \frac{\sigma}{2}\right) \tag{33}$$

where n_{tr} is the number of thrusters in the longest row, σ is the edge-to-edge thruster spacing, and γ was defined in Section III-A, page 3. The thruster spacing σ can be expected to depend on gimbal actuator design and thruster layout. The total translator length is the sum of $2L_a$, and the translator shaft bearing spacing L_b. The bearing spacing, which depends on actuator design and shaft stiffness, can be expected to about equal L_2. Therefore, Eq. (33), the total translator shaft length L_r is

$$L_r = 3.0\, L_d = 1.50\, [n_{tr}\gamma D_b + \sigma(n_{tr} - 1)] \tag{34}$$

The translator shaft mass can now be estimated. It will be assumed that the shafts are tubes with diameters 1/50 of L_r, with wall thickness of about 4×10^{-3} m and density ρ_r. The shaft mass is approximately

$$M_r = 2.5 \times 10^{-4}\, \rho_r L_r^2$$

Substituting for L_r, we obtain

$$M_r = 5.6 \times 10^{-4}\, \rho_r [n_{tr}\gamma D_b + \sigma(n_{tr} - 1)]^2$$

and using Eq. (17), we obtain

$$M_r = 5.6 \times 10^{-4}\, \rho_r \left\{ n_{tr}\gamma \left[\frac{6.30 \times 10^2}{I_{sp}} \left(\frac{\eta_m \eta_t \eta_c P_c}{n_t} \right)^{1/2} \right] + \sigma(n_{tr} - 1) \right\}^2 \tag{35}$$

Translator shaft supports, at the mounting structure and spacecraft interfaces, are expected to weigh about 1 kg per translation axis. Translator shaft bearings are also estimated at 1 kg per axis. For a two-axis system, an additional carriage for carrying the translator actuators is required. This will add about 4 kg.

Actuators are not expected to vary greatly with system size. Gimbal and translator actuators, redesigned from those described in Refs. 17 and 18, weigh 1.8 and 2.7 kg, respectively.

The TVC electronics, which use sun and star sensor input data to derive commands for the actuators, have an estimated weight of about 0.5 kg per actuator.

Thruster mounting-structure mass, including gimbal bearings, is expected to be approximately half the thruster mass. Since the actual value depends entirely on the specific design, this structure mass M_m will be assumed to be

$$M_m = 0.5\, M_t \tag{36}$$

2. Power. The requirements for power can be only approximated at this time. These are shown in Table 3.

Table 3. Power requirements of the thrust vector control elements

Item	Power, W
Electronics,[a] per actuator	1
Translator actuator	14
Driver and stepper motor (13)	
Position pickoff (1)	
Gimbal actuator	9
Driver and stepper motor (8)	
Position pickoff (1)	

[a]Electronics from sun and star sensors to actuator input.

For a three-gimballed thruster, single-axis translator system, the power requirement would be about 45 W. A four-gimballed thruster, two-axis translator system would require about 70 W.

D. Propellant Storage and Distribution

1. Size. An estimate for the size of this element can be obtained by assuming the mass to be a fraction of the

propellant mass. The total propellant flow rate during operation is

$$\dot{M}_p = \frac{7.5 \times 10^{-3} I_b}{\eta_m}, \text{ kg/hr}$$

$$= \frac{7.5 \times 10^{-3} \eta_p \eta_c P_c}{\eta_m V_b}$$

or

$$\dot{M}_p = \frac{7.5 \times 10^{4} \eta_t \eta_c P_c}{I_{sp}^2} \tag{37}$$

where

I_b = total beam current, A

V_b = net beam voltage, kV

The total propellant used is

$$M_p = 7.5 \times 10^4 \int_{t_i}^{t_f} \frac{\eta_t \eta_c P_c}{I_{sp}^2} dt$$

where t_i is propulsion start time, and t_f is finish time. If we now relate M_p to the PSD mass M_{ps} by

$$M_{ps} = \gamma M_p$$

we find that

$$M_{ps} = 7.5 \times 10^4 \gamma \int_{t_i}^{t_f} \frac{\eta_t \eta_c P_c}{I_{sp}^2} dt \tag{38}$$

The factor γ (approximately 0.04) includes tankage, valves, feedlines, and miscellaneous fittings. The integral must be evaluated in mission calculations.

2. Power. Latching valves and pressure transducers are the principal power losses. Each latching value is expected to require a current of 1 A (at 28 V) for about 50 ms.

E. Switching Matrix

The use of switches to interconnect thrusters and PC units may be required to obtain high system reliability. Since the switches with associated drivers and logic are less than 100% reliable, the ultimate incorporation of switches will require a detailed system reliability analysis including accurate data on switch failure rate. These data are unavailable at present.

Both mechanical stepping and solid state (SCR) switches have been considered. Solid state switching is not attractive because of the large voltage drops incurred in high current, low voltage circuits.* The weights of solid state and mechanical switches appear to be comparable.

Switch weight is expected to be about 2.3 kg per PC unit with little dependence on power level or number of thrusters. Switching will occur only with power off. Logic for operating the switches and indicating switch position is estimated at about 1 kg per PC unit.

F. Controller

This unit performs the logic functions related to the thrust subsystem and will probably be a part of the spacecraft central computer and sequencer (CC&S). The principal functions of the controller are to implement the stored thrust program by thruster throttling, to evaluate the available power by scanning the maximum power point detector, to command switching, and to detect thrust subsystem failures. The increment of CC&S weight associated with this unit will be taken as 5 kg. The power required will probably add little to the normal CC&S requirement.

IV. Application

The previous analysis can be illustrated by choosing thruster parameters and number of standby units, and computing the system mass as a function of power level and number of thrusters. It will be assumed that

$\eta_m = 0.90$

$\eta_t = 0.725$ (Fig. 2)

$\eta_c = 0.90$

$n_s = 1$

$n_c = n_t$

$n_p = 0$

$\rho_r = 1.86 \times 10^3$ kg/m^3 (beryllium)

*Personal communication to author from T. W. Macie, JPL, January 1970.

The equations resulting from the use of these parameters are shown in Table 4. Results of calculations based on this table are shown in Figs. 5, 6, and 7 as a function of n_t and P_c for two axes of translation. Similar calculations can be made for other assumed conditions and thruster parameters.

Given curves equivalent to Fig. 7, the mass of a specified configuration can be assessed easily. Thruster throttling and reliability will generally set $(n_t + n_s)$ and mission calculations will set I_{sp} and P_c.

Table 4. Thrust subsystem mass summary

Unit	Mass
Thruster	$M_t = 1.85\,(1 + n_t) + 1.12\left(1 + \frac{1}{n_t}\right) P_c$
PCC	$M_c = (3.7 + 7e^{-0.7P_c/n_t})\,P_c$
TVC	
Two-axis translation	
Translator shafts	$M_r = \left\{1.4\,n_{tr}\left[\frac{630}{I_{sp}}\left(\frac{\eta_m\,\eta_t\,\eta_c\,P_c}{n_t}\right)^{1/2}\right] + 0.05\,n_t\right\}^{1/2}$
Mounting structure	$M_s = 0.5\,M_t$
Translator bearings	2
Translator supports	2
Actuator carriage	4
Electronics	3.7
Translator actuators	5.4
Gimbal actuators	$1.8\,(n_t)$
Propellant storage	$0.5\,P_c$
Switching matrix	$3.3\,n_t$
Controller	5
Wiring	$0.5\,P_c$

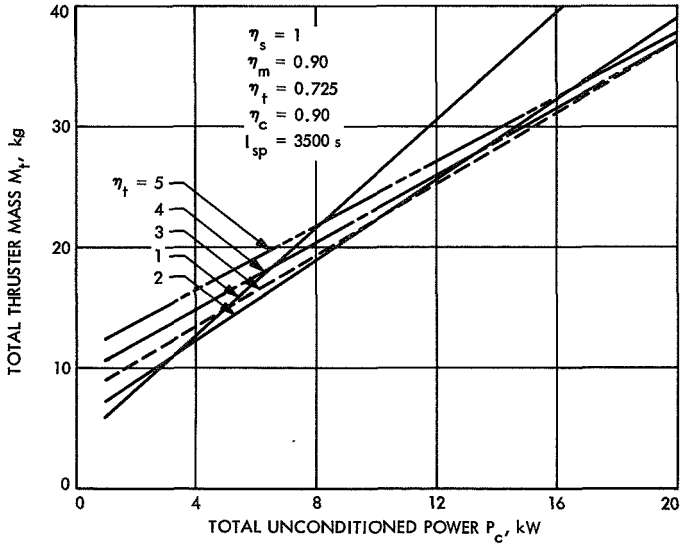

Fig. 5. Total thruster mass for a multi-thruster system

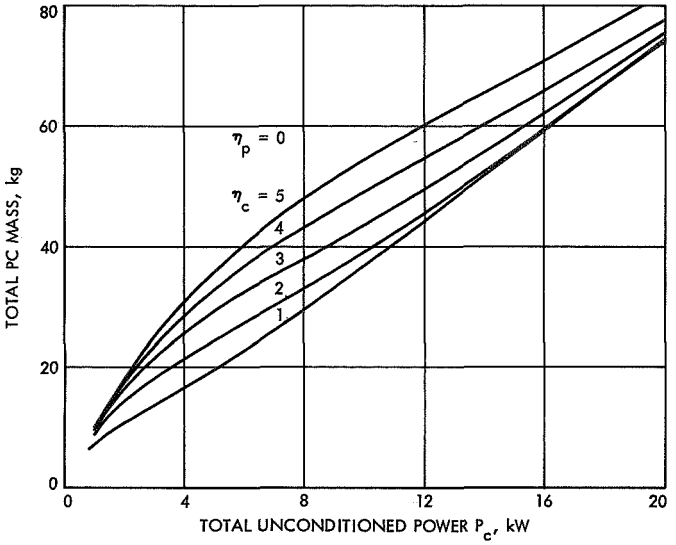

Fig. 6. Total mass of power conditioning and control elements for a multi-thruster system

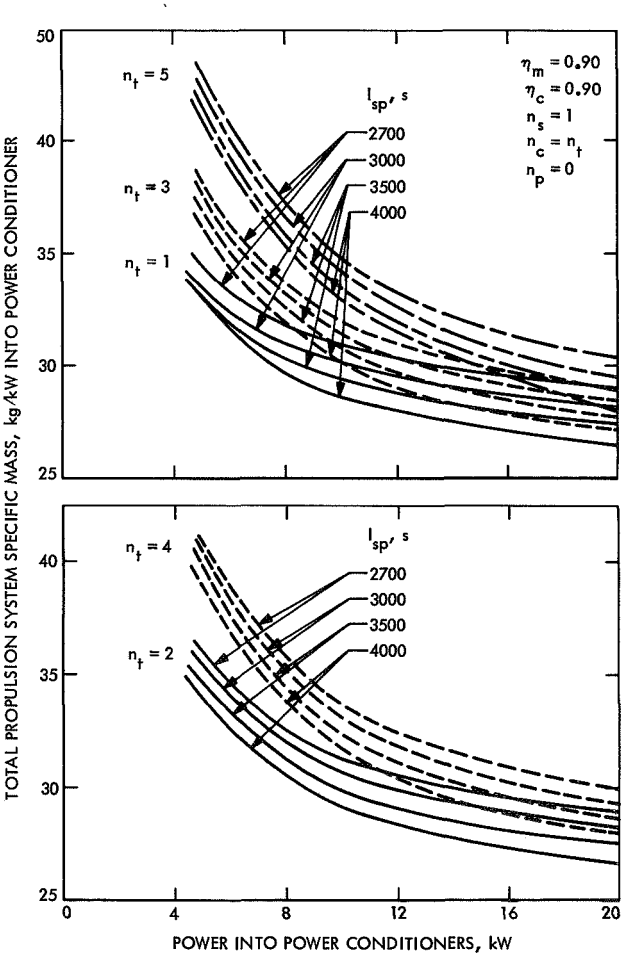

Fig. 7. Total mass of a basic thrust subsystem

References

1. Kerrisk, D. J., and Kaufman, H. R., "Electric Propulsion Systems for Primary Spacecraft Propulsion," Paper 67-424, presented at the AIAA 3rd Propulsion Joint Specialists Conference, Washington, D.C., July 1967.

2. Kerrisk, D. J., and Bartz, D. B., "Primary Electric-Propulsion System Technology and Applications," *Astron. Aeron.*, Vol. 6, No. 6, June 1968.

3. Sandstron, J. D., "Electrical Characteristics of Silicone Solar Cells as a Function of Cell Temperature and Solar Intensity," paper presented at the Third Intersociety Energy Conversion Engineering Conference, Boulder, Colo., Aug. 12–16, 1968.

4. Masek, T. D., "Evaluation of the SE-20C Thruster Design," in *Supporting Research and Advanced Development*, Space Programs Summary 37-51, Vol. III. Jet Propulsion Laboratory, Pasadena, Calif., June 30, 1968.

5. Masek, T. D., and Pawlik, E. V., "Thrust System Technology for Solar Electric Propulsion," Paper 68-541, presented at the AIAA 4th Propulsion Joint Specialist Conference, Cleveland, O., June 1968.

6. Masek, T. D., and Womack, J. R., "Experimental Studies with a Mercury Bombardment Ion Engine System," Paper 67-698, presented at the AIAA Electric Propulsion and Plasma Dynamics Conference, Colorado Springs, Colo., September 1967. Also available as Technical Report 32-1280, *Experimental Studies with a Mercury Bombardment Thrustor System.* Jet Propulsion Laboratory, Pasadena, Calif., July 15, 1968.

7. *Solar Powered Electric Propulsion Spacecraft Study*, Summary Report SSD 60374R. Hughes Aircraft Co., Culver City, Calif., December 1966.

8. Pawlik, E. V., "Performance and Stability of a Hollow Cathode Ion Thruster," in *Supporting Research and Advanced Development*, Space Programs Summary 37-59, Vol. III. Jet Propulsion Laboratory, Pasadena, Calif., October 1969.

9. Bechtel, R. T., "Discharge Chamber Optimization of the SERT II Thruster," Paper 67-688, presented at the AIAA Electric Propulsion and Plasmadynamics Conference, Colorado Springs, Colo., September 1967.

10. Hyman, J., et al., *High Temperature LM Cathode Ion Thrusters*, Final Report on JPL Contract 952131, Hughes Aircraft Co., Research Laboratories, Malibu, Calif., April 1969. Also paper 69-302, presented at the AIAA 7th Electric Propulsion Conference, Williamsburg, Va., March 1969.

11. Pawlik, E. V., and Masek, T. D., "Operation of a 20-cm Diameter Electron-Bombardment Ion Thruster with a Hollow Cathode," in *Supporting Research and Advanced Development*, Space Programs Summary 37-49, Vol. III. Jet Propulsion Laboratory, Pasadena, Calif., Feb. 29, 1968.

12. Sohl, G., Fosnight, V. V., and Goldner, S. J., *Electron Bombardment Cesium Ion Engine System*, Summary Report 6954 on NASA Contract CR-54711. Electro-Optical Systems, Inc., Pasadena, Calif., April 1967.

13. *Low Specific Impulse Ion Engine*, Report 10 on NASA Contract NAS3-11523. Hughes Aircraft Co., Research Laboratories, Malibu, Calif., October 1969.

References (contd)

14. *Electric Thruster Power Conditioner*, First Quarterly Progress Report on JPL Contract. Hughes Aircraft Co., El Segundo, Calif., September 1968.

15. *Multikilowatt Ion Thruster Power Processor*, First Quarterly Report on ERC Contract NAS12-2183. TRW Systems Group, Redondo Beach, Calif., September 1969.

16. Reader, P. D., and Mankovitz, R. J., "Attitude Control of an Electrically Propelled Spacecraft Utilizing the Primary Thrust System," presented at the ASME 1968 Aviation and Space Conference, Los Angeles, Calif., June 1968.

17. Ferrera, J. D., and Perkins, G. S., "Actuator Development for a Clustered Ion Engine Array," in *Supporting Research and Advanced Development*, Space Programs Summary 37-54, Vol. III. Jet Propulsion Laboratory, Pasadena, Calif., December 1968.

18. Perkins, G. S., Johnson, K. G., Ferrera, J. D., and Masek, T. D., *A Mechanism for Three Axis Control of an Ion Thruster Array*, Paper 70-1156, presented at the AIAA 8th Electric Propulsion Conference, Stanford, Calif., August 1970.

19. Macie, T. W., Pawlik, E. V., Ferrera, J. D., and Costogue, E. N., "Solar-Electric Propulsion System Evaluation," Paper 69-498, presented at the AIAA 5th Propulsion Joint Specialist Conference. U.S. Air Force Academy, Colo., June 9–13, 1969.

20. Pawlik, E. V., Macie, T. W., and Ferrera, J. D., "Electric Propulsion Systems Performance Evaluation," Paper 69-236, presented at the AIAA 7th Electric Propulsion Conference, Williamsburg, Va., March 1969.

21. Masek, T. D., and Macie, T. W., *Solar Electric Propulsion System Technology*, Paper 70-1153, presented at the AIAA 8th Electric Propulsion Conference. Stanford, Calif., August 1970.

NASA — JPL — Coml., L.A., Calif.